SUPPLEMENTARY MATERIALS AND METHODS

Embryo perturbation and imaging details

MOs were purchased from Gene Tools; their sequences are listed in Figure S2. The sequence of the control MO is 5'-AGTAGACGAGCTTGTACTGAGGCAT-3'. Injected mRNAs were *in vitro* transcribed using the mMESSAGE mMACHINE kit (Ambion). For Ni and SB treatments, embryos were exposed from fertilization to mesenchyme blastula stage (0-12 hpf). Dose-response experiments were performed to determine the optimal working dose for each reagent presented in this study, and complete descriptions of dose timing and concentration ranges are described in Table S3. Each perturbation experiment was performed in at least three independent biological replicates. From each loss-of-function experiment, a large number of randomly selected plutei were imaged and scored as described in Figure S7. Exemplars were selected for presentation based on the scoring results as those that best reflected the most commonly observed defects for each perturbation. MO phenotypic penetrance data is displayed in Figure S3P.

Skeletal patterning candidate selection rationale

Candidates were selected from an initial list of 879 scaffolds whose expression level (normalized counts) was downregulated in both Ni and SB by ≥ 2-fold compared to control. Of these, 114 genes were identifiable (Table S1). 77 of these encode extracellular proteins (based on orthology), and we manually selected candidates from among this short list. LvSLC26a2/7 was selected because of its orthology to a mammalian skeletal patterning gene (Mount and Romero, 2004). LvNFL (Notch- and Fibropellin-like) was selected because of its probable adhesive functions (Bisgrove et al., 1991), which we reasoned are likely to contribute to ectodermal patterning mechanisms. LvLOX (lipoxygenase) was selected because LOX-produced HETEs regulate a range of signaling pathways (Pidgeon et al., 2007). Finally, LvBMP5-8 was selected because it is a well-known signaling ligand, and because it was upregulated by Ni and SB in the initial assembly, and therefore reflected a mutually upregulated candidate.

Candidate gene cloning, sequence, and splice analysis

Candidate gene sequence reads were used to assemble provisional gene models, which were empirically extended by RACE using FirstChoice RLM-RACE kit (Ambion). Intron positions were predicted based on corresponding intron positions in S. purpuratus ((Sodergren et al., 2006), http://www.echinobase.org), then amplified, cloned and sequenced for splice-blocking MO sequence design. Phylogenetic analysis was performed using MrBayes (http://mrbayes.sourceforge.net) and visualized using FigTree (http://tree.bio.ed/ac/uk/software/figtree/). Sequence alignment was carried out using MultAlin (Corpet, 1988). Full length LvSLC26a2/7 cDNA (GenBank accession number KR055815) was obtained by RACE, then subcloned into pCS2 for in vitro transcription, after the addition of an artificial polyA track (20mer) in the 3' UTR to enhance mRNA stability *in vivo*. LvNFL (GenBank accession number KR055816), LvBMP5-8 (GenBank accession number KT428770), and LvLOX (GenBank accession number KR055817) cDNAs were cloned using standard methods and subcloned into pCS2 for in vitro transcription. For RT-PCR splice analysis, total RNA from control, SLC MO-, NFL MO- and BMP5-8 MO-injected embryos at LG stage was collected and DNase-treated using the RNeasy Micro Kit (QIAGEN), and cDNAs were synthesized using the Transcriptor High Fidelity cDNA Synthesis Kit (Roche). Relevant primer sequences are listed in Table S4.

Alcian Blue signal quantitation and pseudocoloring, and Cuprolinic acid staining

Scoring of Alcian blue-stained embryos was restricted to embryos photographed in posterior views to optimize dorsal and ventral signal comparisons. Gray scale images were analyzed in ImageJ, which was used to select multiple regions of interest (ROIs) in the ectoderm. The average pixel intensity per unit area was determined for each ROI. Three or four independent ventral and dorsal ROIs were averaged per embryo, then their ratios were calculated. For pseudocoloring, gray scale images were generated, then a custom rainbow look up table was applied that colors pixel intensities according to the scale presented in Figures 3 and S6 using the software Canvas (ACD Systems). Fixation and Cuprolinic acid staining were simultaneously performed in 2.5% gluteraldehyde (Polysciences, Inc.) with 0.025 M sodium cacodylate (Sigma), 2.5 M $MgCl_2$ (MP Biomedicals), and 1% Cuprolinic blue cationic dye (Quinolinic phthalocyanine; Polysciences, Inc.) in ASW for approximately 90 minutes at room temperature to label sulfated proteoglycan side chains (Chan et al., 1992); embryos were then washed, imaged, and pseudocolored as described for Alcian blue.

Table S1

Click here to Download Table S1

Table S2

Click here to Download Table S2

Table S3. Perturbation timing and dose information

Perturbation (Vendor)	Stage (hours post fertilization, hpf)	Dose Range
$NiCl_2$ (Sigma)	Zygote to 12 hpf	0.3 mM – 0.5 mM
SB203580 (Calbiochem)	Zygote to 12 hpf	25 µM – 30 µM
LvSLC26a2/7 MO (Gene Tools)	Zygote	1.33 mM - 2.67 mM
LvSLC26a2/7 mRNA	Zygote	1.25 µg/µl – 4 µg/µl
LvNFL MO (Gene Tools)	Zygote	1 mM – 2 mM
LvNFL mRNA	Zygote	12 – 14 µg/µl
LvBMP5-8 MO (Gene Tools)	Zygote	0.5 mM – 1.33 mM
LvBMP5-8 mRNA	Zygote	0.5 – 1 µg/µl
LvLOX MO (Gene Tools)	Zygote	0.53 mM – 0.8 mM
LvLOX mRNA	Zygote	1 – 2 µg/µl
Control MO (Gene Tools)	Zygote	1 mM
Sulfur-free artificial sea water	10 hpf	0 mM magnesium sulfate
Sodium chlorate (Sigma)	10 hpf	10 mM – 30 mM
High sulfate artificial sea water	10 hpf	68 mM – 100 mM magnesium sulfate
Axitinib (Sigma)	16 hpf	25 nM

Table S4. Primer sequences

Primer	Sequence (5' --> 3')	Use
LvSLC26a2/7 forward	TAGATGATCGAACGGAGGACC	cloning
LvSLC26a2/7 reverse	CAATCCAATTAAGGGTTTCGAGTTGTTTGC	cloning
LvSLC26a2/7 5' UTR BamHI	atcaaggatccCAGTGCCATGGACCACTGGATTGC[a]	cloning
LvSLC26a2/7 3' UTR polyA XhoI	atatactcgagttttttttttttttttttttCACCAAGAATT ATCCCCGTCC[a]	cloning
LvSLC26a2/7 splice analysis forward (exon 13)	GTGGATCTTGGTCTTGGTGTCG	splice analysis
LvSLC26a2/7 splice analysis reverse (exon 14)	CTGTCTGAACTGCTGGGCATTGG	splice analysis
LvSLC26a2/7 splice analysis reverse (exon 16)	GGTTGCTATGCCAATCCTGTCG	splice analysis
LvNFL forward HindIII	attaagcttCCACCACCAAACCTGCCACACG[a]	cloning
LvNFL reverse XbaI	atatctagaCCCGATGTTCGGAAGTAAATTGCAGG[a]	cloning
LvNFL splice analysis forward (exon L)	ACTGGAGTCACGTGTGAGACG	splice analysis
LvNFL splice analysis reverse (exon M)	ACCATTTCGACACGGATTGC	splice analysis
LvNFL splice analysis reverse (exon O)	CACGTAGCATCAACTTGACAGG	splice analysis
LvBMP5-8 start EcoRI	ggaattcATGCTCATTTTCCCTTCAGTGATG[a]	cloning
LvBMP5-8 stop XhoI	ccgctcgagCTAAAGGCAACCACAGGCACG[a]	cloning
LvBMP5-8 splice analysis forward (exon 1)	TTGGACCAGGGCTAAGTTGG	splice analysis
LvBMP5-8 splice analysis reverse (exon 2)	GAGGTATCCTACCGATGTCG	splice analysis
LvBMP5-8 splice analysis reverse (exon 3)	CCTGAGATGGGATGAAGTCG	splice analysis
LvLOX stop XbaI	ccgtctagaTTAAATACTGATTGCATTAGGGACTTCTTTAGG[a]	cloning
LvSLC26a2/7 forward	TCCCTGTTGGATTTCCCAAAC	qPCR
LvSLC26a2/7 reverse	CACTGCAAAGCCCACAATAGC	qPCR
LvVEGF forward	CTACAAAGGAAGGCGGAACG	qPCR
LvVEGF reverse	GCTCCGTTGATACATGGTGG	qPCR
LvVEGFR forward	CCACCATCACCCATCAAACCACC	qPCR
LvVEGFR reverse	CCCTGACCTGAATCCACTGG	qPCR
LvPax2/5/8 forward	CGGCTGTTGGCCGAGGGTGTGTGC	qPCR
LvPax2/5/8 reverse	CGTCCTCTCTGGGTCTCCAGGGTG	qPCR
LvWnt5a forward	CGAGCTCTTCATCCTTGGTACA	qPCR
LvWnt5a reverse	TGGTCCTGGTAGAGCTGACATA	qPCR
LvUnivin forward	CAAATGGCAGCAACAGAAGA	qPCR
LvUnivin reverse	GGAATGGAAGCTACGTCGAA	qPCR
LvSetmar forward	GCCATCATGTCCTTGTCTCA	qPCR
LvSetmar reverse	CACATGAAGCTTGATCAGGTAGTC	qPCR

[a]Upper case indicates gene-specific sequence, while lower case indicates artificial polyA track (underlined) and restriction sites.

REFERENCES

Bisgrove, B. W., Andrews, M. E. and Raff, R. A. (1991) 'Fibropellins, products of an EGF repeat-containing gene, form a unique extracellular matrix structure that surrounds the sea urchin embryo', *Developmental Biology* **146**(1): 89-99.
Chan, F. L., Inoue, S. and Leblond, C. P. (1992) 'Localization of heparan sulfate proteoglycan in basement membrane by side chain staining with cuprolinic blue as compared with core protein labeling with immunogold', *Journal of Histochemistry and Cytochemistry* **40**(10): 1559-72.
Corpet, F. (1988) 'Multiple sequence alignment with hierarchical clustering', *Nucleic Acids Research* **16**(22): 10881-90.
Mount, D. B. and Romero, M. F. (2004) 'The SLC26 gene family of multifunctional anion exchangers', *Pfluegers Archiv European Journal of Physiology* **447**(5): 710-21.
Pidgeon, G. P., Lysaght, J., Krishnamoorthy, S., Reynolds, J. V., O'Byrne, K., Nie, D. and Honn, K. V. (2007) 'Lipoxygenase metabolism: roles in tumor progression and survival', *Cancer and Metastasis Reviews* **26**(3-4): 503-24.
Sodergren, E. Weinstock, G. M. Davidson, E. H. Cameron, R. A. Gibbs, R. A. Angerer, R. C. Angerer, L. M. Arnone, M. I. Burgess, D. R. Burke, R. D. et al. (2006) 'The genome of the sea urchin Strongylocentrotus purpuratus', *Science* **314**(5801): 941-52.

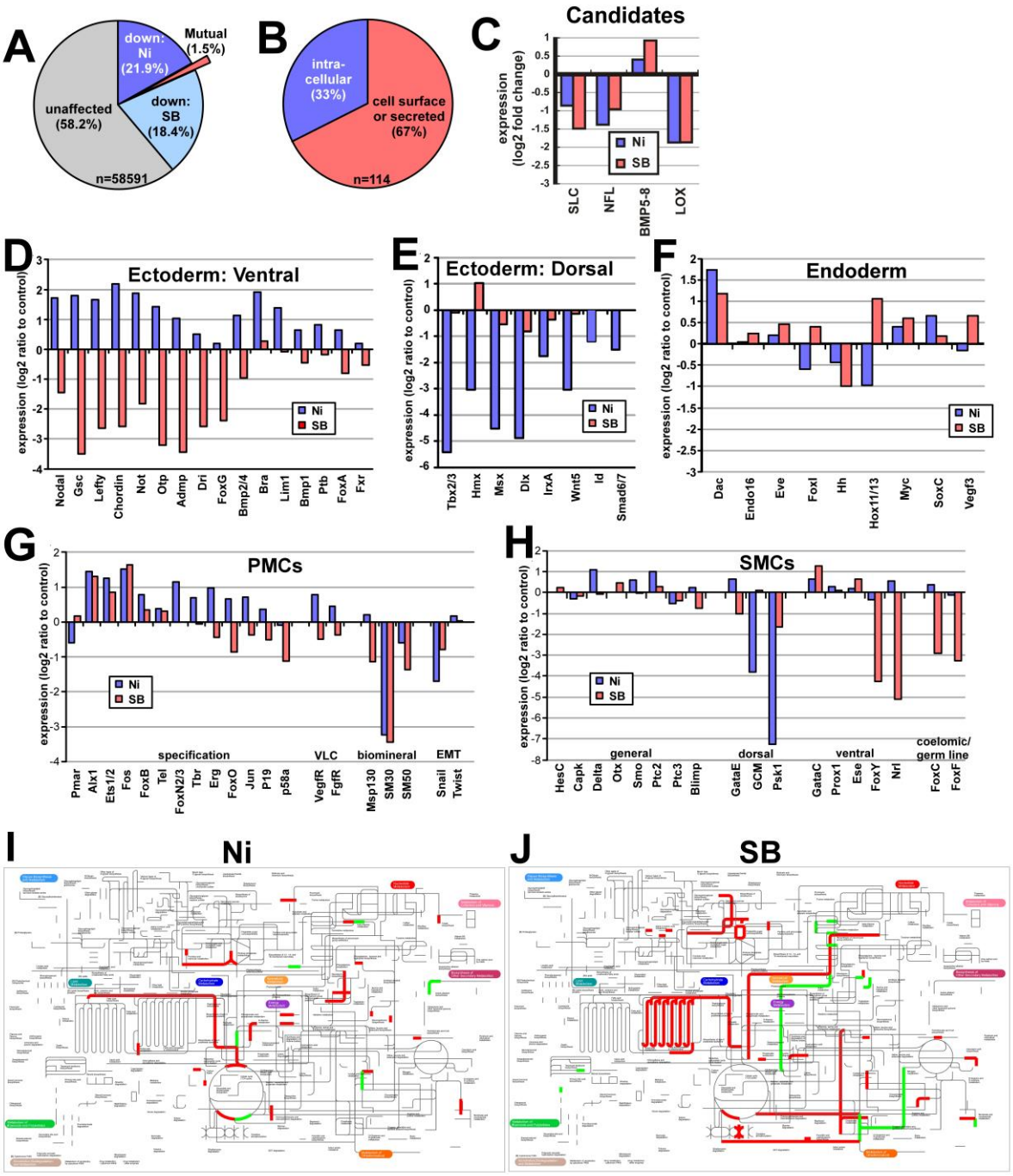

Figure S1. Identification of skeletal patterning candidates by differential analysis of RNA-Seq data and expression analysis of known specification, differentiation, and metabolic genes. A-B. Pie charts display the results of the differential expression analysis from the initial assembly. From the mutually downregulated set (A; red), the subcellular distribution of the identifiable subset is shown (B). **C.** RNA-seq expression values from the final assembly are shown relative to controls for the four candidate skeletal patterning genes described in Fig. 2. **D-H.** RNA-seq expression values from the final assembly are shown relative to controls for genes specifically expressed in the ventral ectoderm (D), the dorsal ectoderm (E), the endoderm (F), the skeletogenic primary mesenchyme cells (PMCs; G), and the secondary mesenchyme cells (SMCs; H). **I-J.** Differential RNA-seq expression values for 372 sea urchin metabolic network components were mapped using iPath 2.0. Increased (green) and decreased (red) gene expression at a 4-fold cut-off is shown for Ni (I) and SB (J) at late gastrula stage compared to controls.

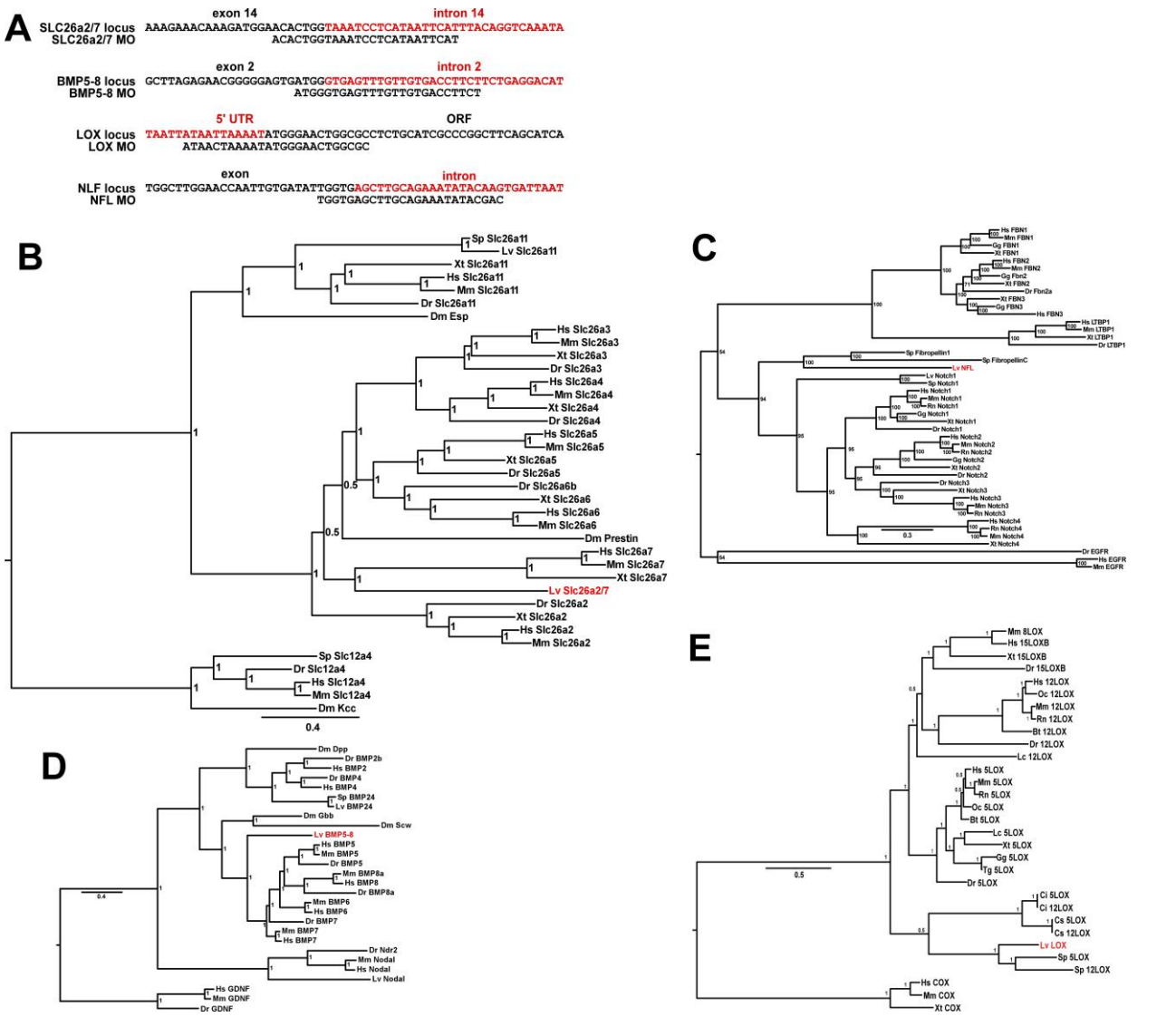

Figure S2. Morpholino design and phylogenetic analysis for four identified skeletal patterning candidate genes. A. The designs for morpholino antisense oligonucleotide (MOs) sequences are shown for six skeletal patterning candidate genes. Three MOs are designed to block mRNA splicing (SLC, BMP5-8, and NFL), while one is designed to block translation (LOX). Untranslated sequences are indicated in red. **B-E.** Phylogenetic analysis for SLC (B), NFL (C), BMP5-8 (D), and LOX (E) are shown as distance trees produced by Bayesian inference, with node probabilities shown, and candidates indicated in red. Species included are echinoderm: Lv, *Lytechinus variegatus*; Sp, *Strongylocentrotus purpuratus*; vertebrate: Hs, *Homo sapiens*; Mm, *Mus musculus*; Rn, *Rattus norvegicus*; Oc, *Oryctolagus cuniculus*; Gg, *Gallus gallus*; Xt, *Xenopus tropicalis*; Dr, *Danio rerio*; Bt, *Bos taurus*; Lc, *Latimeria chalumnae*; Tg, *Taeniopygia guttata*; invertebrate chordate: Ci, *Ciona intestinalis*; Cs, *Ciona savignyi*; and arthropod: Dm, *Drosophila melanogaster*.

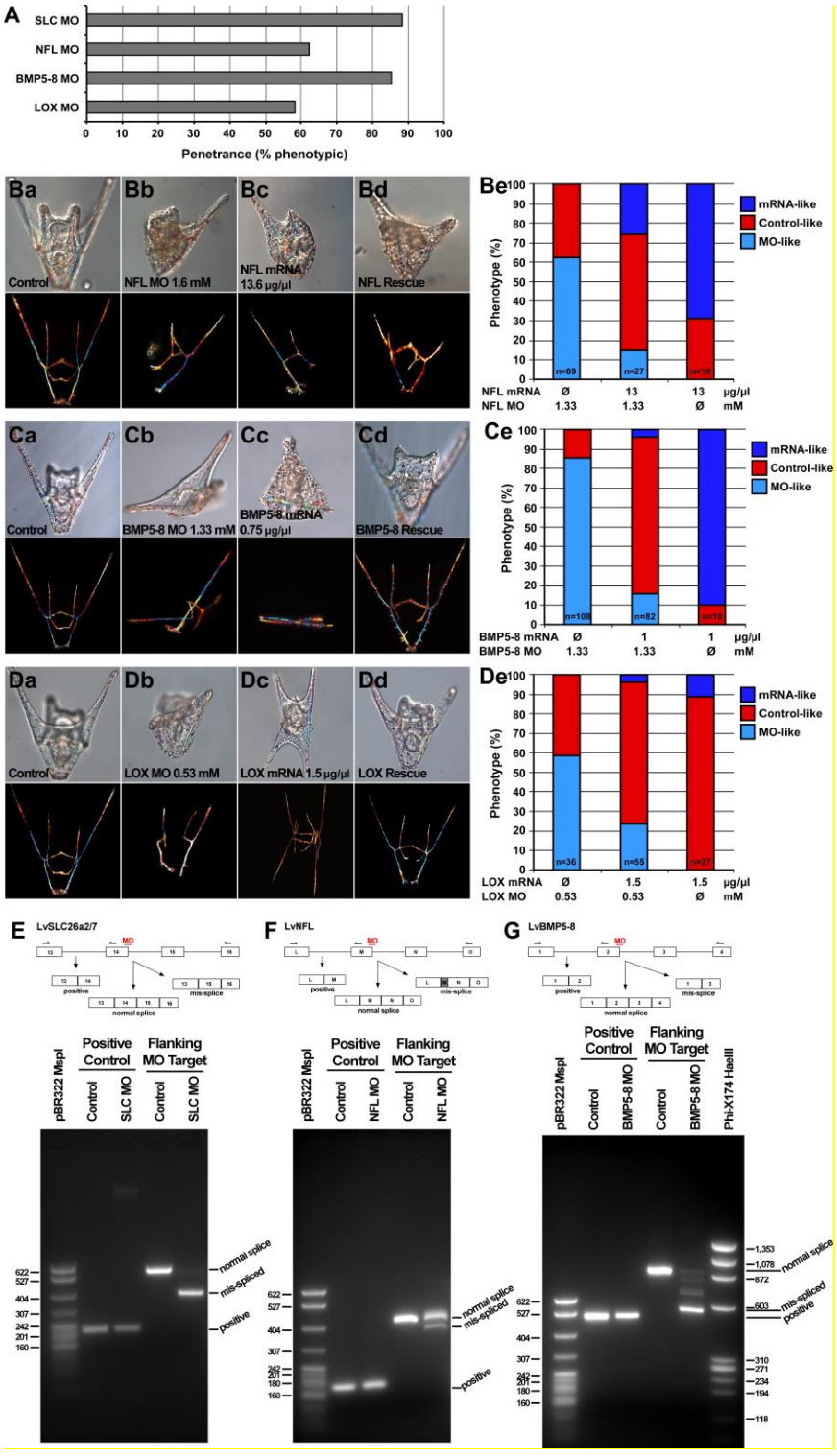

Figure S3. Skeletal patterning gene MOs are specific. A. Penetrance of SLC, NFL, BMP5-8 and LOX MOs as determined by percent of phenotypic embryos. **B-D.** Rescue experiments were performed for NFL (D), BMP5-8 (E), and LOX (F). Exemplar phenotypes are shown for control, LOF, GOF and rescued plutei by DIC (upper panels) and skeletal images (lower panels), and quantitated to determine reproducibility (De, Ee, Fe). MO and mRNA doses for rescued plutei are indicated in the graphs. See Figure 3T-3Y for SLC MO specificity controls. **E-G**. Splice analysis for control, SLC MO- (1.33 mM; E), NFL MO- (1 mM; F), and BMP5-8 MO-injected (2 mM; G) embryos at LG stage, showing an amplicon upstream the MO target site ("positive control") and another that spans the MO target site ("flanking MO target") as indicated in the schematics.

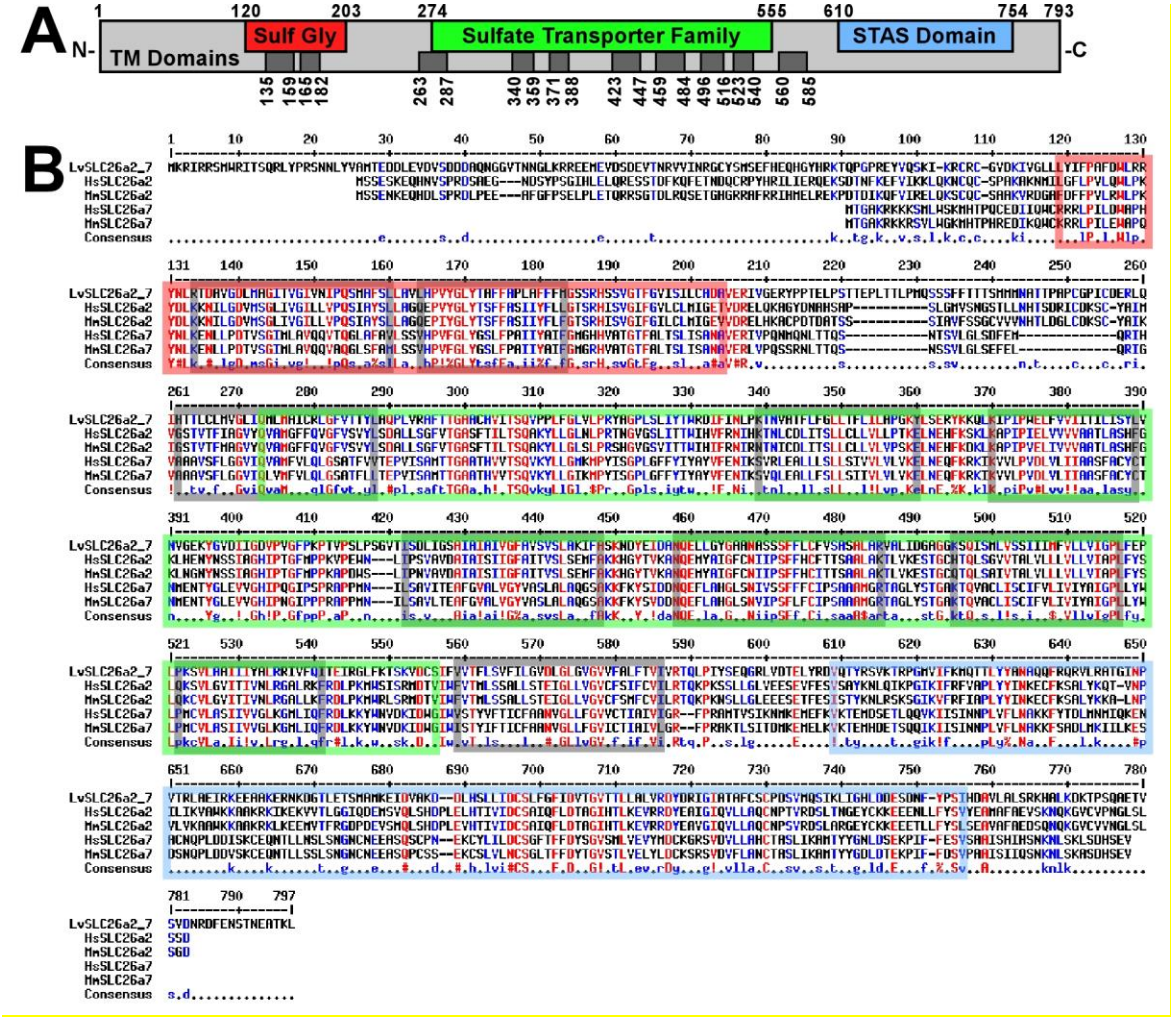

Figure S4. Sequence analysis indicates that LvSLC26a2/7 is most similar to vertebrate SLC26a2 and SLC26a7 genes. A. LvSLC26a2/7 conserved domains include Sulf Gly (sulfate transporter N-terminal domain with GLY motif, red), Sulfate Transporter Family (green), and STAS (sulfate transporter and anti-sigma factor antagonist, blue). Predicted transmembrane domains are indicated as dark grey boxes. Amino acid numbers above and below the schematic indicate domain boundaries. **B.** Predicted LvSLC26a2/7 amino acid sequence alignment with Hs and Mm SLC26a2 and SLC26a7 translations are displayed with conserved domains boxed, following the color scheme in A.

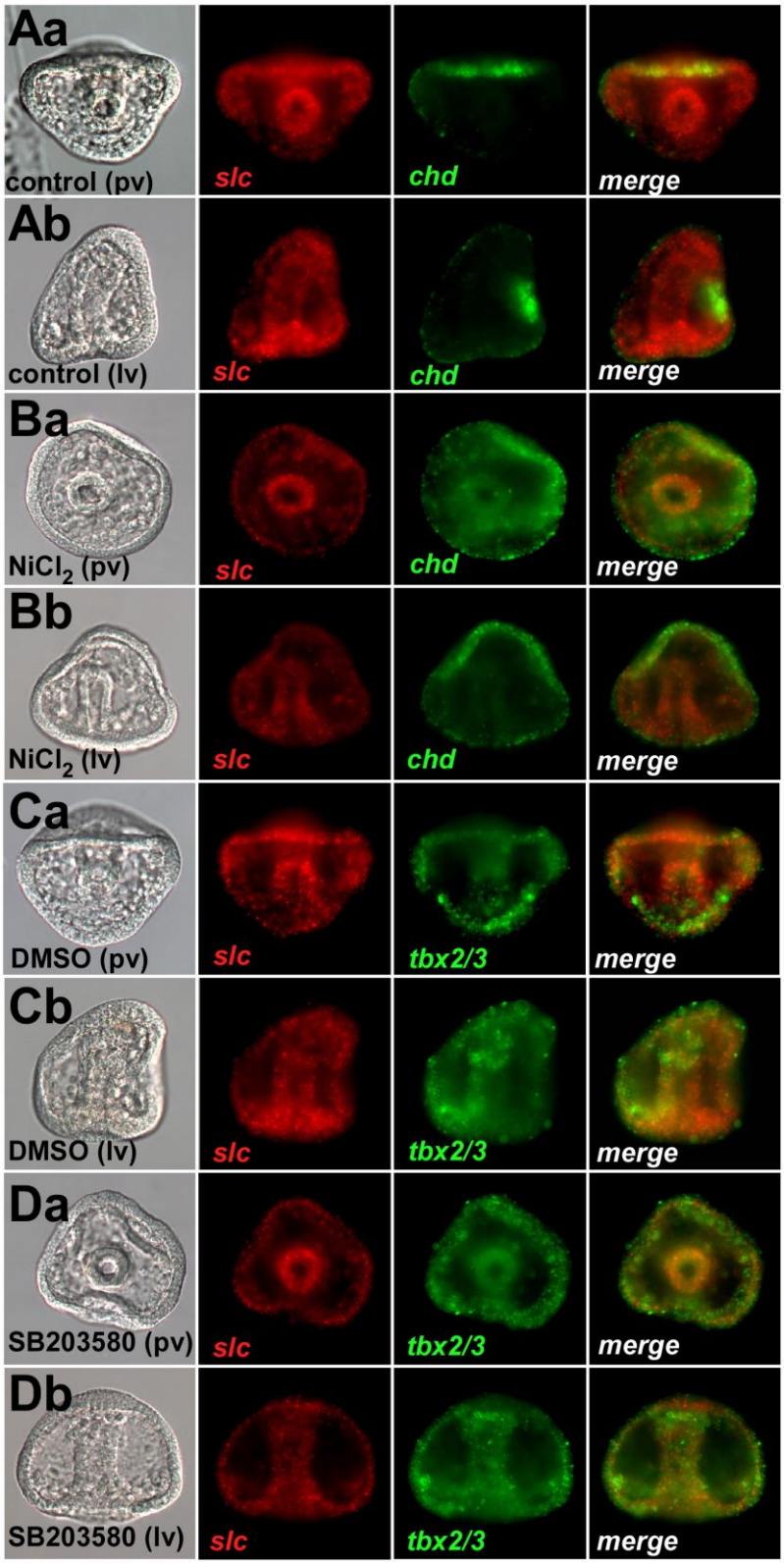

Figure S5. LvSLC26a2/7 expression is suppressed in sea urchin embryos treated with Ni or SB. Fluorescent *in situ* hybridization for *slc26a2/7* (*slc,* A-D, red) and either ventrally-expressed *chordin* (*chd*) (A-B, green), or dorsally-expressed *tbx2/3* (C-D, green) in untreated (A) or vehicle-treated (DMSO; C) controls, or in Ni- (B) or SB- (D) treated embryos at late gastrula stage, in posterior views (pv; Aa,Ba,Ca,Da) and lateral views (lv; Ab,Bb,Cb,Db).

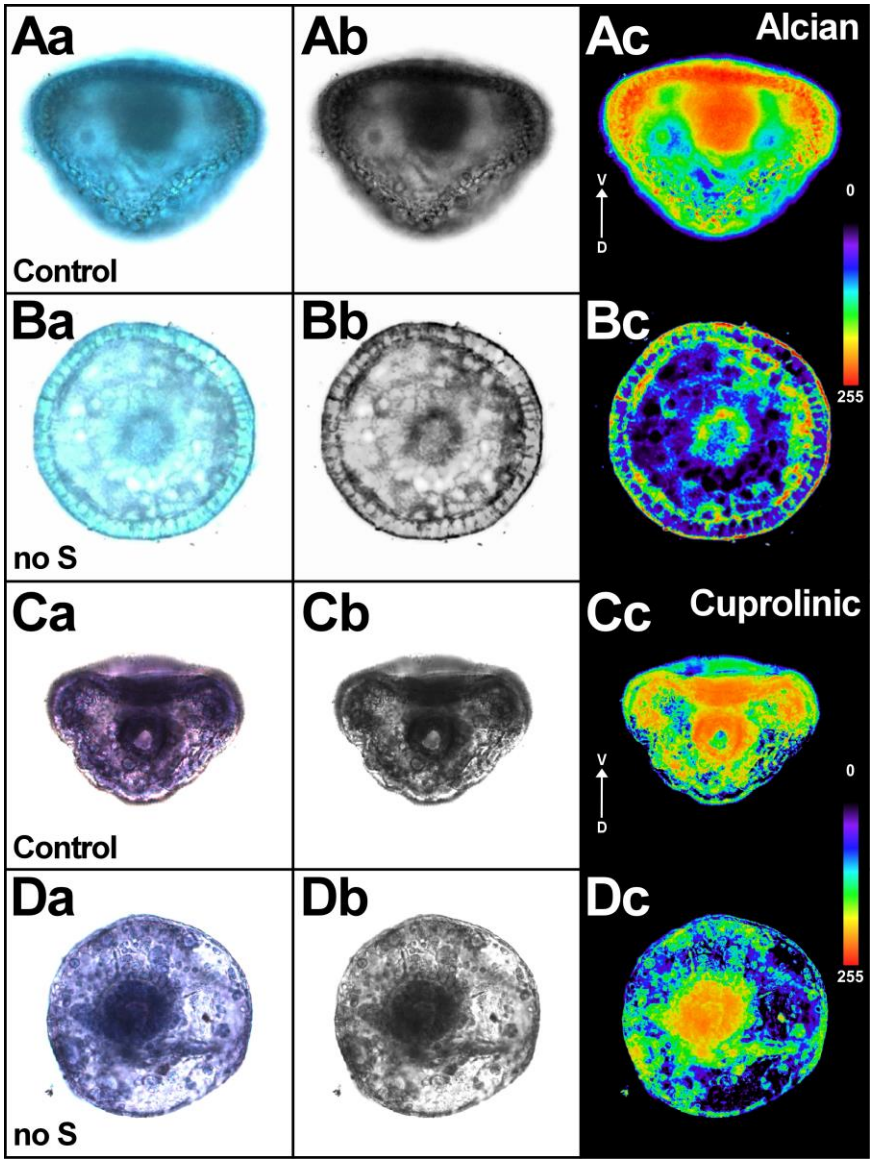

Figure S6. Alcian blue and Cuprolinic acid staining highlights ventral SPG accumulation in control embryos. Control embryo (A,C) and embryo cultured in sulfur free sea water (B,D) at LG stage were stained with Alcian blue (A,B) under SPG-specific conditions, or with Cuprolinic acid (C,D). Raw images (a) were converted to gray scale and subjected to histogram normalization (b), then a custom rainbow look up table (insets) was applied (c). The dorsal-ventral axis is indicated. Note that the fixation conditions for Cuprolinic acid results in shrinking of the embryo.

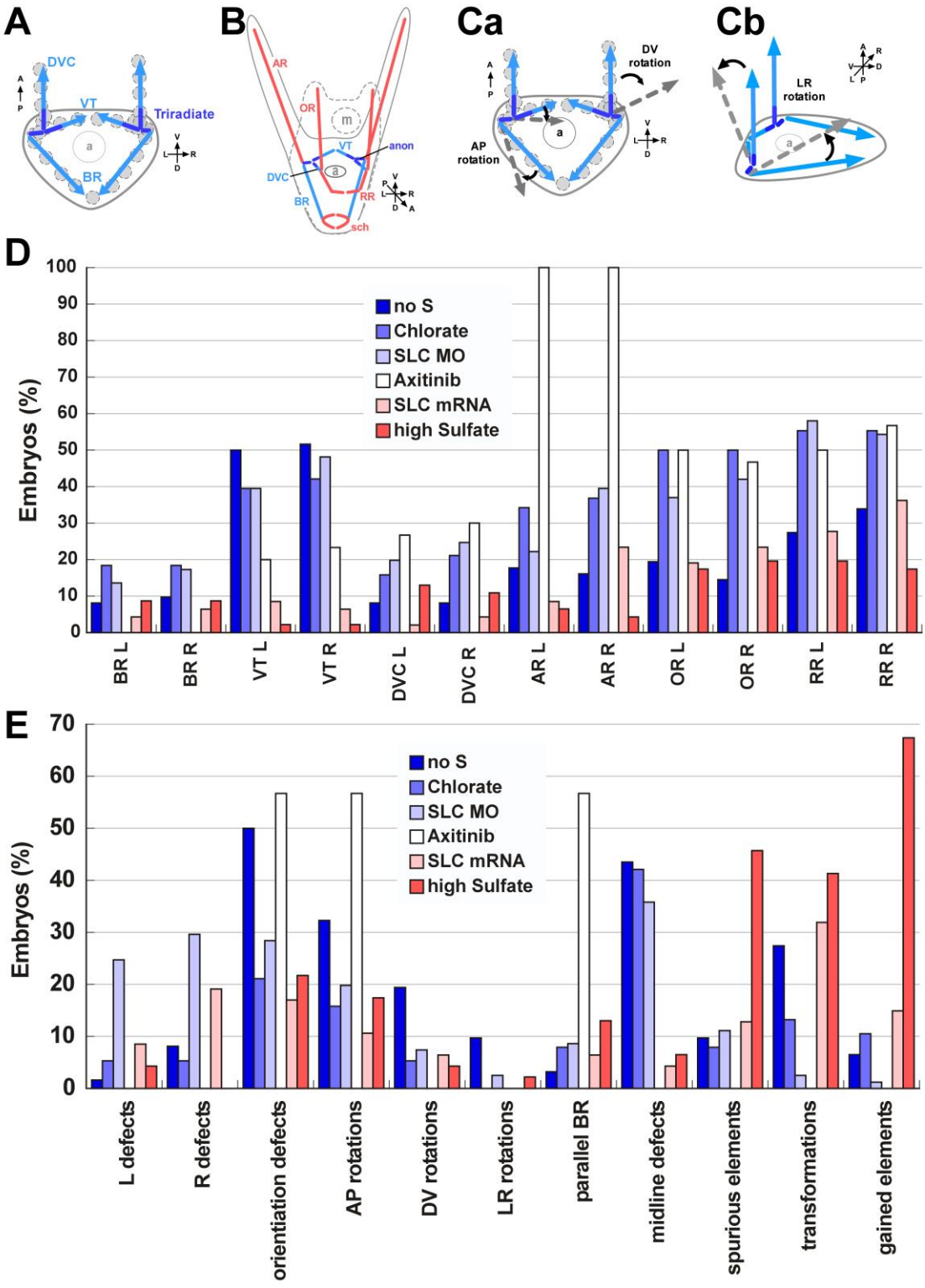

Figure S7. Skeletal scoring analysis highlights significant skeletal patterning defects in sea urchin embryos. **A.** Schematic displaying the primary skeleton at late gastrula stage. The initial triradiates (dark blue) in the ventrolateral PMC clusters extend into the ventral PMC ring to produce the ventral transverse rods (VTs), into the PMC cords to produce the dorsoventral connecting rods (DVCs), and laterally to produce the anonymous rods (anon), which extend only slightly before branching. The primary skeletal elements (light blue) also include the

body rods (BRs), which branch from the anonymous rods and extend into the dorsal PMC ring. The anus (a) is indicated. **B.** Schematic depicting the skeleton at pluteus stage. Here, the secondary skeleton is indicated in red, and includes the posterior anal rods (ARs), which branch ventrally from the anonymous rods, the posterior scheitel (sch), which branches from the dorsal tips of the body rods, and the anterior oral rods (ORs) and recurrent rods (RRs), which branch from the dorsoventral connecting rods (DVCs). Production of the secondary skeleton requires PMC migration out of the initial ring-and-cords pattern. The anus (a) and mouth (m) are indicated. **C.** We developed a skeletal patterning scoring rubric, which included scoring losses and gains for the elements shown in B, as well as a range of additional defects including left and right side-biased losses, midline defects, spurious elements, element transformations, and skeletal orientation defects. We classified orientation defects as rotations about the anterior-posterior (Ca), dorsal-ventral (Ca), or left-right (Cb) axis. Some embryos exhibited more than one orientation defect. Midline defects are defined as the absence of skeletal elements from the left-right midline of the pluteus (i.e., short or absent VTs and RRs, and absent sch). Spurious elements are defined as elements present where no element would normally develop, while gained element refers to duplications of normal rods. For rotational defects, embryos were counted if at least one element was appropriately perturbed, while LR defects were counted for an LR imbalance of at least two rods. In cases where the presence of an element was ambiguous because of the orientation of the embryo, we assumed the element was present. **D-E.** The frequency of skeletal patterning defects, with left (L) and right (R) side elements scored independently for pluteus stage larvae following SLC/SPG perturbation (no S, Chlorate, SLC MO, SLC mRNA, high Sulfate) or VEGF inhibition (Axitinib). Skeletal losses (D) and additional defects (E) are shown. Data are depicted as the percentage of embryos exhibiting each defect. Sample sizes are: no S, 62; chlorate, 38; SLC MO, 81; axitinib, 30; SLC mRNA, 47; high sulfate, 46. Fig. 3 and Fig. 5 depict selected portions of these results. Uninjected controls (n=34) and GST MO-injected controls (n=18) show normal skeletal development in 100% of the embryos, and are not graphically displayed.

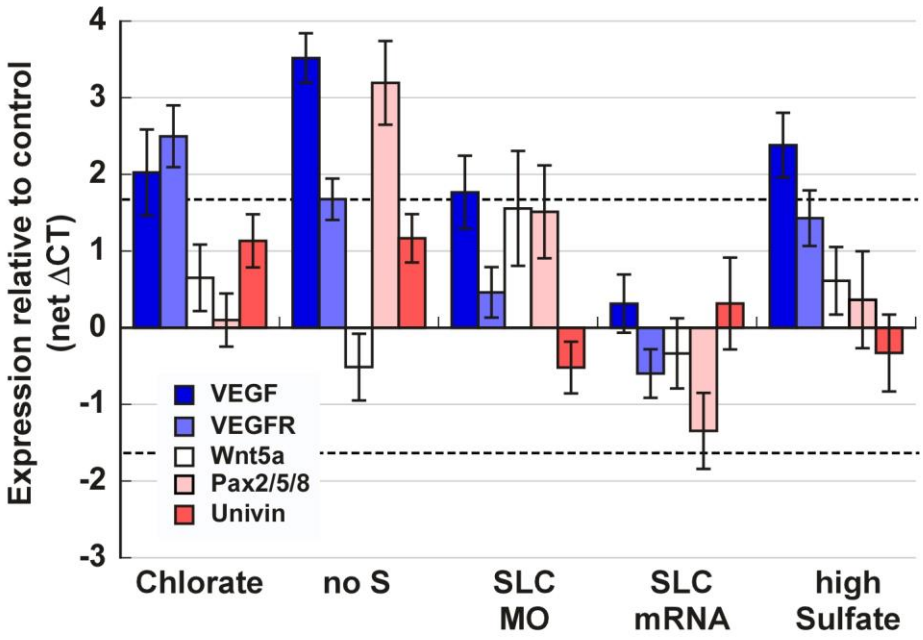

Figure S8. VEGF and/or VEGFR expression level is upregulated by SLC/SPG perturbations.
The expression of VEGF, VEGFR, Wnt5a, Pax2/5/8, and Univin relative to controls was determined by qPCR at late gastrula stage following SLC/SPG perturbations described in Figures 3 and 4. The results are displayed as normalized ΔC_T values ± s.e.m. Dashed lines indicate the threshold of significance at ΔC_T of 1.7 (approximately 3-fold).